Journal of Photochemistry & Photobiology, A: Chemistry 462 (2025) 116258

Contents lists available at ScienceDirect

Journal of Photochemistry & Photobiology, A: Chemistry

journal homepage: www.elsevier.com/locate/jphotochem

Optical nonlinearity of *Tectona Grandis L.f.* (teak) leaf extract under continuous wave and pulsed laser excitation

Beryl C. [a,b,*], Amogh M.S. [a,b], Cyril Benny [a,c], P.R. Biju [b], Reji Philip [a]

[a] Ultrafastand Nonlinear Optics Lab, Light and Matter Physics Group, Raman Research Institute, Bangalore 560080, India
[b] Schoolof Pure & Applied Physics, M.G. University, University Campus Rd, Athirampuzha, Kerala 686560, India
[c] Institute of Physics, University of Rostock, Albert-Einstein-Str.23, 18059 Rostock, Germany

ARTICLE INFO

Keywords:
Tectona Grandis L.f. (teak)
Natural dye
Z-scan
Nonlinear absorption
Nonlinear refraction
Optical limiter

ABSTRACT

In this work, we investigate the linear and nonlinear optical properties of the natural dye obtained from *Tectona Grandis L.f.* leaves by solvent extraction. *Tectona Grandis L.f.* of the Verbenaceae family, which provides high-quality, high-value timber for various uses, is a major strategic element in the forestry economies of many tropical countries. We investigated the nonlinear optical properties at 532 nm using CW and pulsed (5 ns) lasers, employing the techniques of Z-scan and Spatial Self phase modulation (SSPM). Theoretical fits to the measured data under CW excitation give the third-order nonlinear absorption coefficient (β_{eff}) in the order of 10^{-3} cm/W, and the nonlinear refractive index coefficient (n_2) in the order of 10^{-6} cm^2/W, respectively. The β_{eff} and n_2 values obtained for pulsed excitation are in the order of 10^{-8} cm/W, and 10^{-15} cm^2/W, respectively. These values are comparable to those of efficient nonlinear optical (NLO) materials previously reported in literature, revealing the applicability of the teak leaf extract natural dye in optical limiting applications for protecting sensitive optical detectors and human eyes from hazardous laser radiation.

1. Introduction

Nonlinear optical (NLO) properties of materials are of special interest in the areas of optical communications, optical storage, optical computing, harmonic generation, optical switching, and optical power limiting[1–10]. NLO properties of organic dyes such as chlorophyll, carotenoids, betanin, etc. have attracted substantial research interest in the past [11–13]. Natural dyes can be extracted from bio-resources like fruits, vegetables, roots, leaves, bark, and micro-organisms[14–17]. They are environment-friendly and cost-effective. The nonlinear transmission mechanism in most of these dyes depend on reverse saturable absorption (RSA) arising from excited state absorption.

In this work, we investigate nonlinear absorption and refraction of the natural dye extracted from *Tectona Grandis L.f.* (teak) leaves. Teak is a prominent source of high-quality, high-value timber, playing a strategic role in the forestry economies of many tropical regions. In commercial teak plantations, annual branch pruning is essential to achieve the desired tree form suitable for timber extraction. While the woody portions of the tree are extensively utilized in the timber industry, the pigmented leaves are often discarded as agricultural waste. We have used the dye extracted from young, pigmented teak leaves as the sample for this research. The techniques of Z-scan[18,19] and Spatial Self Phase Modulation (SSPM) are used for the determination of both nonlinear absorption coefficient (β_{eff}) and nonlinear refractive index coefficient (n_2). The experiments are carried out at 532 nm wavelength using CW and pulsed (5 ns) lasers with varying input powers and energies, respectively. Results show that the dye has potential applications in the fabrication of optical limiters, which can be employed for the protection of human eyes and sensitive optical detectors from accidental exposure to hazardous levels of laser radiation.

2. Materials and methods

Tender leaves of *Tectona Grandis L.f.* were collected, washed thoroughly, sun-dried for a week, and then crushed into powder form. The powder was then mixed with Dimethyl sulfoxide (DMSO) and refrigerated below 4 °C for 24 h for maximal extraction of the dye. The colloidal solution thus obtained was then centrifuged for 10 mins at 6000 rpm. The supernatant was collected and filtered using grade 4 Whatman filter paper to get an optically clear liquid of reddish-brown color, which was then stored in the refrigerator at a low temperature of 4 °C for the measurements.

* Corresponding author.
E-mail address: beryl1983@gmail.com (B. C.).

https://doi.org/10.1016/j.jphotochem.2024.116258
Received 7 November 2024; Received in revised form 21 December 2024; Accepted 30 December 2024
Available online 2 January 2025

Ultraviolet–Visible (UV–Vis) absorption spectrum of the sample was measured using a spectrophotometer (Lambda 35, Perkin Elmer). Excitation and emission spectra were measured using a spectrofluorometer (Fluromax 4, Horiba Jobin-Yvon). FTIR was taken using SHIMADZU FTIR-IR TRACER 100.

3. Linear optical Studies

3.1. Uv–vis Spectroscopy

According to literature reports, Tectona Grandis L.f. extract contains about 50 different compounds[20–23]. The UV–Vis absorption spectrum of the extract in DMSO is shown in Fig. 1. The extract exhibited broad absorption in the range 400—700 nm, with absorption bands peaking at 433 nm and 663 nm respectively. These peaks confirm the presence of chlorophyll *a* [24,25]. The absorption seen in the green region of the spectrum (from 500 to 600 nm), corresponds to the anthocyanin pigment[26,27].

3.2. Photoluminescence (PL) spectra

The PL spectrum of the teak leaf extract was recorded using the excitation wavelength of 350 nm (Fig. 2). The spectrum shows a broad, intense emission arising from chlorophyll *b* and anthocyanin pigments in the region 400 nm – 550 nm, with the peak at 432 nm corresponding to emission from anthocyanin [28]. The major emission of chlorophyll *a* monomers peaks at 672 nm, followed by a weak shoulder in the region 700 – 750 nm (the sharp small peak observed at 700 nm is the second-order diffraction of the excitation wavelength). Solvatochromic data can be used to determine $\pi \rightarrow \pi^*$ and $n \rightarrow \pi^*$ spectroscopic transitions. If there is a bathochromic (red) shift with increasing solvent polarity, then it can be confirmed that the transition is $\pi \rightarrow \pi^*$[29]. Both peaks exhibit a bathochromic shift with increasing solvent polarity (DMSO > DMF > Ethanol) in our case, indicating a HOMO-LUMO ($\pi \rightarrow \pi^*$) transition (please see supplementary information).

3.3. IR spectra

Fig. 3 shows the FTIR spectrum of the dye in the range 500 cm^{-1} to 4000 cm^{-1}. The spectrum shows a broad absorption in the range 3700 cm^{-1} to 3100 cm^{-1} with two strong peaks at 3423.65 cm^{-1} and 3415.93 cm^{-1}, which are related to the –OH stretching of anthocyanin and chlorophyll dyes respectively. The small peaks at 2999.31 cm^{-1} and

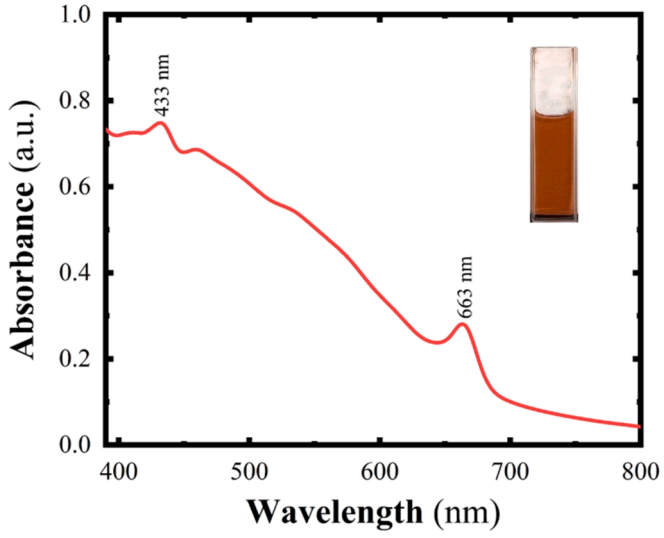

Fig. 1. UV–vis absorption spectrum of *Tectona Grandis L.f.* leaf extract in DMSO.

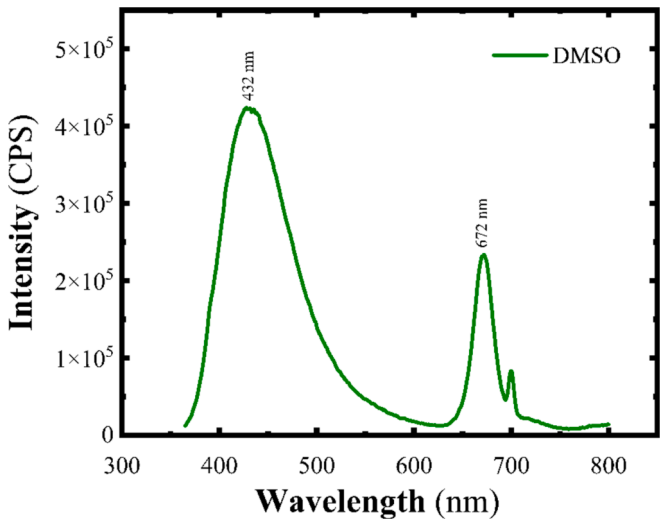

Fig. 2. Emission spectrum of the *Tectona Grandis L.f.* dye, measured at the excitation wavelength of 350 nm.

2914.44 cm^{-1} are associated with the symmetric and antisymmetric –C–H– stretching vibrations of CH_2 and CH_3 groups, respectively. C = O (ester/ketone/aldehyde) bonds vibrate at 1658.78 cm^{-1} (ketonic bonds of chlorophyll vibrate at ~ 1700 cm^{-1}). The peaks at 1436.97 cm^{-1} and 1406.11 cm^{-1} correspond to the asymmetric bending of CH_3 (δsCH_3), and the peak at 1311.59 cm^{-1} is identified as a symmetric deformation of CH_3 (δsCH_3) group that is attached to the S atom[30]. The sharp peak at 1016.49 cm^{-1} is the aromatic ring C-H deformation[31]. The peak at 952.84 cm^{-1} corresponds to aromatic C-H in-plane bend, and peaks at 671.23 cm^{-1} and 665.44 cm^{-1} indicate alkyne C-H bend. The peak at 468.7 cm^{-1} indicates aryl disulfides (S-S stretch)[32]. The FTIR spectra reveal the existence of C = O, C-H, and C-O bonds that contribute to coloring components dye indicating the existence of anthocyanin [33,34].

4. Nonlinear optical studies

4.1. Z-scan

We employed both open and closed-aperture Z-scan[18] techniques (Fig. 4), for measuring the imaginary and real parts of the complex nonlinear refractive index, respectively. The Z-scan is a simple and efficient single-beam method with sensitivity comparable to that of interferometric methods[18,19]. It allows simultaneous determination of the sign and magnitude of absorptive as well as refractive nonlinearities associated with a material medium, and hence, can differentiate between the contributions of real and imaginary parts of the third order nonlinear susceptibility $\chi^{(3)}$.

A low power CW diode laser, and an Nd:YAG laser emitting 5 ns pulses, were used as light sources. Both lasers emitted radiation at 532 nm. The beam was focused using a plano-convex lens of focal length 10 cm. The concentrated dye extract was diluted with DMSO to give different linear transmission (LT) values at 532 nm as required. Samples were taken in a 1 mm cuvette, which was mounted on a stepper-motor-controlled linear translation stage and placed in the beam path. The sample was moved over a total distance of 15 mm in steps of 50 μm each and the transmittance was measured at each step. For CW excitation the transmitted laser power was measured using a laser power meter (Thorlabs), and for pulsed excitation the transmitted energy was measured by a pyroelectric detector (Rjp 735, Laser Probe Corp.). The movement of the translation stage, the firing of the laser, and data acquisition were controlled by a Python program. For performing the closed aperture Z-scan, an aperture of suitable diameter was placed in

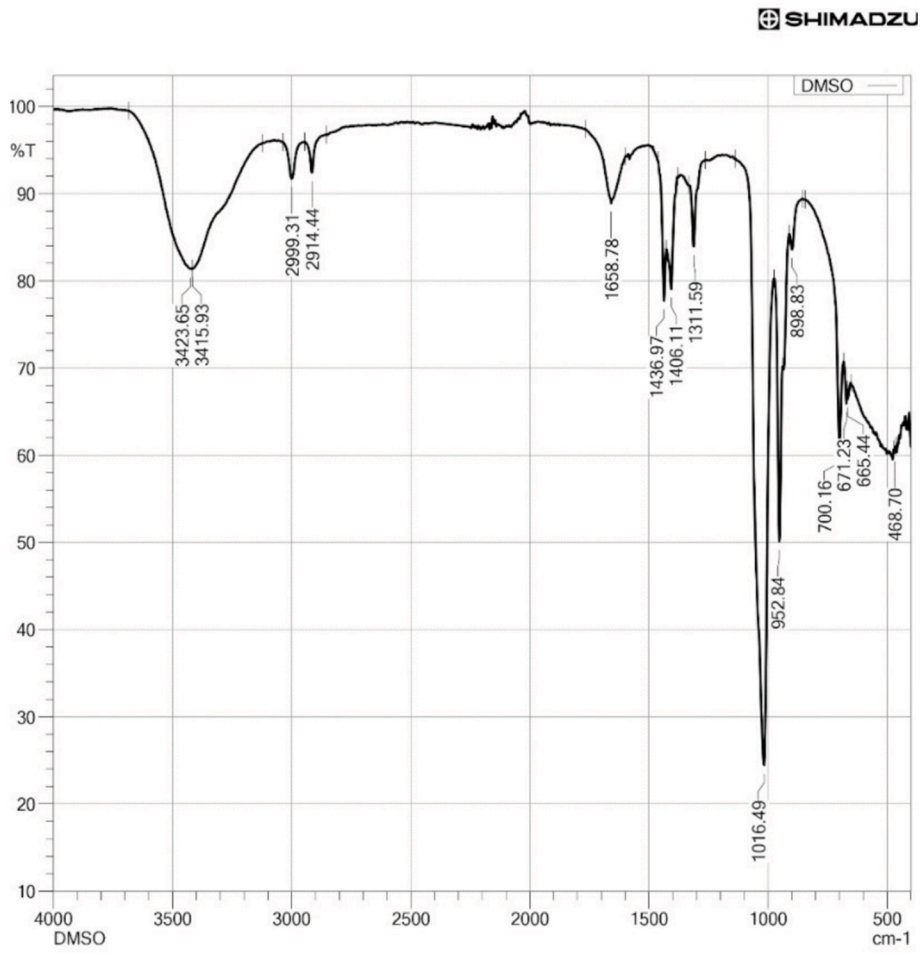

Fig. 3. FTIR spectrum of *Tectona Grandis L.f.* dye in DMSO.

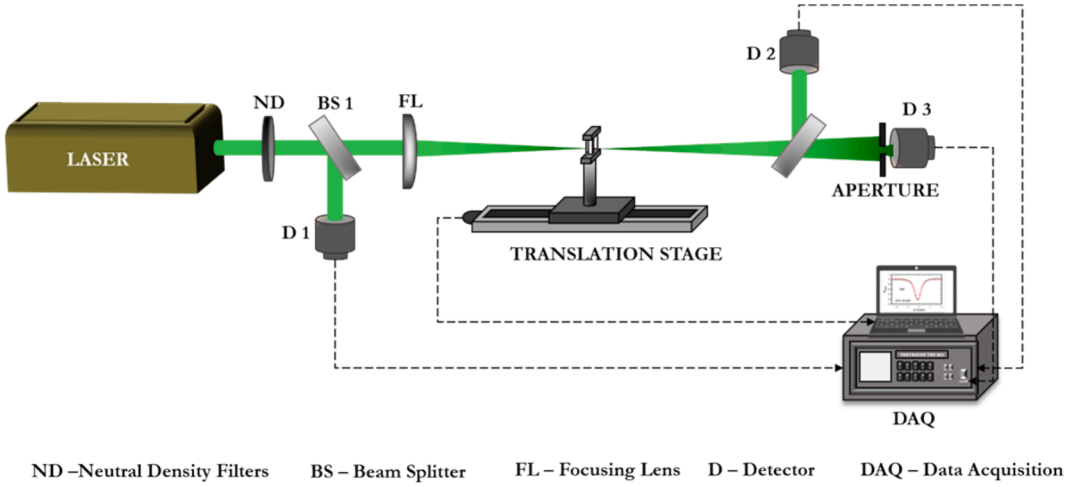

Fig. 4. Experimental set up for the automated closed aperture Z-scan experiment. For open aperture measurements the aperture in front of D3 is removed. Beam focus is designated as $z = 0$.

front of the detector[19] to provide an aperture linear transmittance (S) of 0.5. The beam waist radius at the focal point (ω_0) was calculated to be 17 μm, and the corresponding Rayleigh length, given by

$$z_R = \frac{\pi\omega_0^2}{\lambda} \quad (1)$$

was found to be 1.71 mm for our experiment. z_R is larger than the sample thickness, which is a requirement for Z-scan measurements[35].

It is possible to plot the sample transmission T(z) against input laser intensity $I_{in}(z)$ using the open aperture Z-scan data. For this we note that for a spatially Gaussian beam, the optical fluence $F_{in}(z)$ at any position z can be calculated from the corresponding beam radius $\omega(z)$ and the input laser pulse energy E_{in}. The beam radius is given by

$$\omega(z) = \omega(0)\left[1 + \left(z/z_R\right)^2\right]^{1/2} \quad (2)$$

and the position-dependent fluence can be calculated from the expression,

$$F_{in}(z) = \frac{4(\log 2)^{1/2} E_{in}}{\pi^{3/2}\omega(z)^{1/2}} \quad (3)$$

The corresponding intensity is given by

$$I_{in}(z) = \frac{F_{in}(z)}{\tau} \quad (4)$$

where τ is the laser pulse width.

4.1.1. Open aperture Z-scan

In the open aperture scheme, the transmitted intensity (I_{out}) for a given input intensity (I_{in}) can be calculated from the expression

$$I_{out}(z) = I_{in}(z)\exp -\left[\left(\frac{\alpha_0}{1+\left(\frac{I}{I_s}\right)}\right) + \beta_{eff} I\right] \quad (5)$$

with the transmission,

$$T(z) = \frac{I_{out}(z)}{I_{in}(z)} \quad (6)$$

Here α_0 is the linear absorption, I_s is the saturation intensity, and β_{eff} is the third order nonlinear absorption coefficient, which accounts for the excited state absorption taking place in the medium. I_s and β_{eff} can be numerically obtained from the experimental data using equations (2) to (6).

A diode laser was used for performing CW Z-scan measurements. One of the open aperture Z-scans measured for the dye solution is given in Fig. 5(a) and the corresponding nonlinear transmission curve is given in Fig. 5(b). In this case as the sample approaches the focus the transmittance decreases; this behaviour is known as Reverse Saturable Absorption (RSA). In organic dye molecules RSA occurs when excited state absorption (ESA) is stronger than ground state absorption. Materials showing strong RSA are called “optical limiters”. When the intensity of input light increases the transmittance of an optical limiter will decrease, making it more opaque. This property of optical limiters is useful for protecting human eyes and sensitive optical detectors from accidental damage caused by powerful laser beams. The strength of RSA in a material increases with the value of the third order nonlinear absorption coefficient β_{eff} given in Equation (5).

Fig. 6 (a) shows the variation of β_{eff} with input laser power. β_{eff} is found to increase with the laser power, for the samples with LT values of 50 % and 60 %. The β_{eff} values obtained are in the order 10^{-3} cm/W, which is comparable to the values reported in literature[36](Table 1). β_{eff} values of the sample calculated from the Z-scan curves by fitting the experimental data to eqn. (5), plotted as a function of linear absorption coefficient (α_0), are shown in Fig. 6 (b). β_{eff} is found to increase with α_0, which indicates that the increased population in the excited state resulting from a higher α_0 leads to enhanced nonlinear absorption.

Open aperture Z-scans measured for the dye solution using pulsed excitation (7 ns laser pulses) are given in Fig. 7(a)-(i). The sample shows RSA behaviour. Fig. 8 shows the variation of β_{eff} with laser pulse energy and sample linear absorption coefficient, and Table 2 lists the values.

The RSA behaviour seen in Fig. 7 results from the excited state absorption (ESA) process[37] occurring in the present samples. For some samples weak shoulder peaks can be seen (e.g., Fig. 7e and 7 h), which arise from absorption saturation occurring at moderate input intensities (accounted for by the term I_s in Eqn. (5))[38,39]. As a macroscopic parameter that depends on the concentration of nonlinearly absorbing molecules, β_{eff} can be expressed as $\sigma_2 N/h\nu$, where σ_2 is the nonlinear absorption cross-section of the material, $h\nu$ is the photon energy, and N is the number density of molecules in the system[35]. Obviously, β_{eff} will increase with N (and also with α_0). ESA is a strong process due to the involvement of real intermediate states, resulting in a relatively large σ_2 value. Since σ_2 will depend on population re-distribution among the electronic states, β_{eff} will become a function of input intensity as well [40]. It is worthwhile here to consider the role of genuine two-photon absorption (2PA) in the observed nonlinearity. 2PA is a weak process as it involves virtual intermediate states, and its contribution to the measured RSA will be much smaller as compared to that of ESA in the present case.

4.1.2. Closed aperture Z-scan

To obtain the nonlinear refractive index, closed aperture Z-scan was carried out in the sample solution. Fig. 9 (a) shows the Z-scan curves obtained at 70 % linear transmittance using 3 mW laser power. Variation in transmittance (Δ T) with distance was measured in the range of −25 mm to 25 mm around the focal point. The peak-valley shape of the closed aperture Z-scan curve implies that the sample exhibits self-defocusing type of non-linearity (negative n_2). When nonlinear absorption is weak the transmittance curve obtained in closed-aperture configuration will show a symmetric peak and valley structure. The transmittance is proportional to the phase shift and Rayleigh length (z_R) as follows:[41]

$$\Delta T(z) = 1 + \frac{\Delta\varphi_0\, 4x}{(x^2+1)(x^2+9)} \quad (7)$$

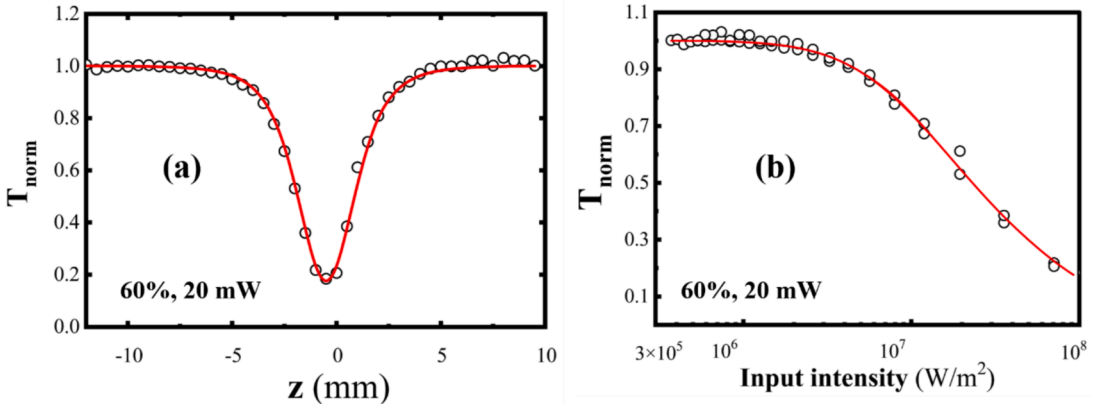

Fig. 5. (a): Open aperture Z-scan measured for the dye under CW excitation. LT of the sample is 60 %, and the laser input power used is 20 mW. **(b):** Normalized transmission vs. Input intensity, calculated from the open aperture Z-scan data.

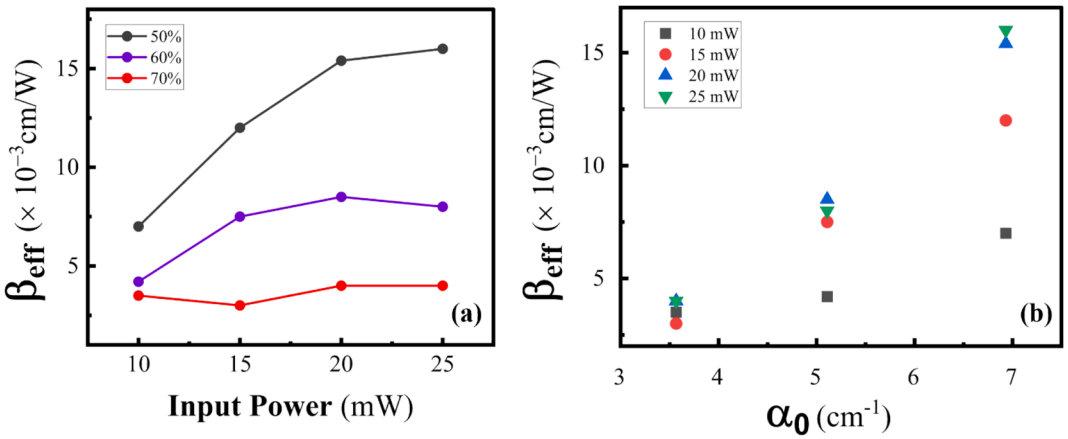

Fig. 6. (a): Variation of β_{eff} with laser power, for samples having LT values of 50%, 60%, and 70%, respectively. **(b)**: β_{eff} plotted as a function of the linear absorption coefficient (α_0) for different laser powers.

Table 1
The nonlinear absorption coefficient β_{eff} and other parameters for the samples excited using CW laser.

Linear Transmission (LT)	α_0 (cm^{-1})	Laser power (mW)	β_{eff} ($\times 10^{-3}$ cm/W)
50 %	6.93	10	7
		15	12
		20	15.4
		25	16
60 %	5.11	10	4.2
		15	7.5
		20	8.5
		25	8
70 %	3.57	10	3.5
		15	3
		20	4
		25	4

where $\Delta\varphi_0$ and x are the phase change and normalized distance, respectively. The normalized distance is given by $x = z/z_R$.

By fitting the data points in Fig. 9(a) to Eqn. (7), the the value of $\Delta\varphi_0$ can be determined. The nonlinear refractive index (n_2) can then be found from the expression

$$n_2 = \frac{\Delta\varphi_0}{KL_{eff}I_0} \tag{8}$$

where I_0 and $k = 2\pi/\lambda$ are the on-axis irradiance at focal point, and the wave vector, respectively. L_{eff} is the effective length of nonlinear medium, given by

$$L_{eff} = \left(\frac{1 - e^{-\alpha_0 L}}{\alpha_0}\right) \tag{9}$$

where α_0 is the linear absorption coefficient. The n_2 values obtained are given in Table 3.

From Table 3 it is clear that the magnitude of n_2 increases with sample concentration and decreases with laser power. Under CW irradiation the refractive nonlinearity is mostly thermal in nature. This is confirmed from the observations that all the closed aperture Z-scan curves show a peak-valley separation of $\approx 2Z_R$. A peak-valley separation of more than 1.7 times the Rayleigh range (Z_R) is a clear indication of thermal nonlinearity[42]. The increase in n_2 for lower linear transmittance values is due to the prominence of thermal nonlinearity at higher concentration. Materials which show excited state absorption (ESA) normally exhibit excited state refraction as well; this is a consequence of the redistribution of population that alters the absorption spectrum, which by causality, modifies the refractive index[43]. In addition, increasing laser power increases thermal absorption, which raises the material's temperature and reduces the refractive index. Such sample heating results in thermal lensing, as in the present case. For gases, the refractive index consistently decreases with rising temperature (at constant pressure), while in condensed matter, it may either increase or decrease depending on the material's internal structure. This likely explains the decrease in the nonlinear refractive index observed in our system with increasing laser input power. Thermal effects with CW laser excitation develop over relatively long timescales, often on the order of seconds, making the nonlinear refractive index time-dependent [44].

Fig. 10 (a)-(l) show closed aperture Z-scans measured for samples having different concentrations, at different laser energies. The sign of the nonlinear refraction is negative and its magnitude is found to decrease linearly with intensity. When the nonlinear refraction coexists with nonlinear absorption in a material, the transmittance curve for CA Z-Scan exhibits a suppressed peak and an enhanced valley. The Z-scan curve is asymmetric in this case. The asymmetry depends on a parameter $\rho = \chi_I^{(3)}/\chi_R^{(3)}$, which is the ratio of the imaginary part of the third order susceptibility to the real part.

Under the thin-sample, small aperture, and low-irradiance limits, the normalized transmittance $\Delta T(z)$ in CA Z-Scan is given as[45],

$$\Delta T(z) = 1 + \frac{4x}{(x^2+1)(x^2+9)}\Delta\varphi_0 - \frac{2(x^2+3)}{(x^2+1)(x^2+9)}\Delta\Psi_0 \tag{10}$$

with

$$\Delta\varphi_0 = Kn_2L_{eff}I_0 \tag{11}$$

and

$$\Delta\Psi_0 = \frac{\beta L_{eff}I_0}{2} \tag{12}$$

Introducing the coupling factor $\rho = \chi_I^{(3)}/\chi_R^{(3)}$, the equation can be rewritten as,

$$\Delta T(z) = 1 + \frac{2(-\rho x^2 + 2x - 3\rho)}{(x^2+1)(x^2+9)}\Delta\varphi_0 \tag{13}$$

This equation was used to fit the measured data shown in Fig. 10 (a)-(l). The values of ρ and n_2 are given in Table 4.

The suppressed peak and enhanced valley are a clear indication of the contribution of nonlinear absorption in addition to the thermal contributions. The thermal effect consists of two processes in which one is the "fast" process of acoustic wave propagation, and the other is the "slow" steady state changing of medium density due to accumulative thermal heating of the absorbing area. The slow process should be taken into consideration in the case of low thermal conductivities and/or high

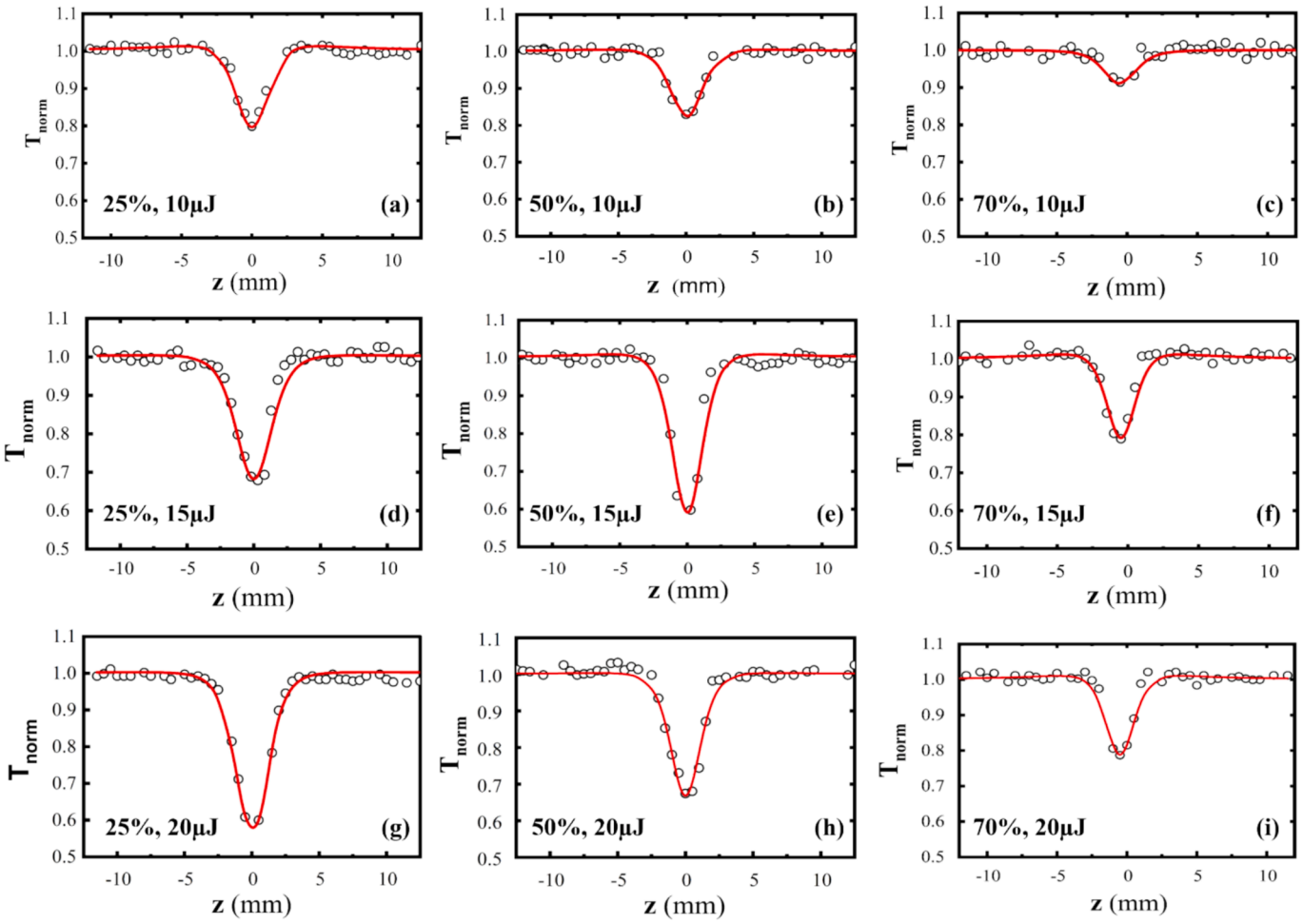

Fig. 7. (a)-(i): Open aperture Z-scan curves measured for the dye under 7 ns pulsed excitation. LT values of the samples are 70 %, 50 %, and 25 %, respectively. Laser pulse energies used are 10, 15, and 20 µJ, respectively.

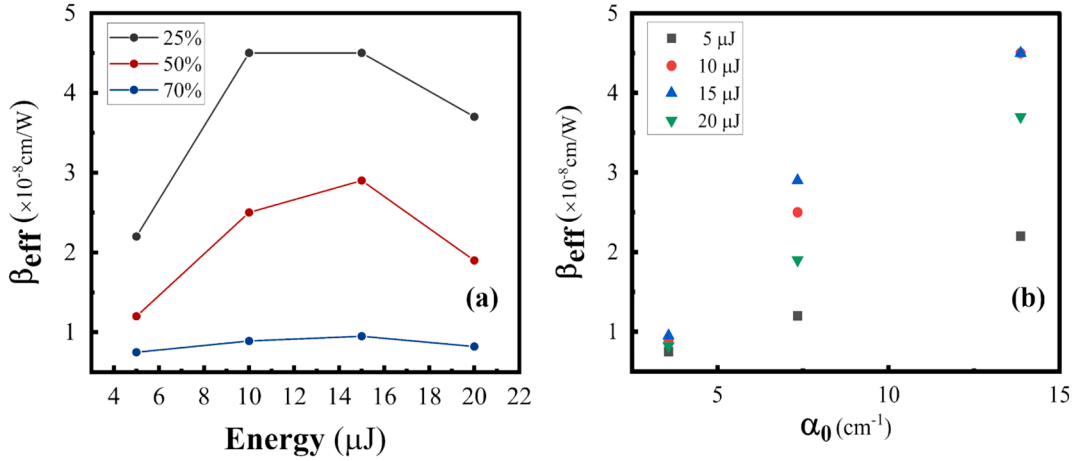

Fig. 8. Variation of β_{eff} with **(a)** energy of the laser pulse, and **(b)** linear absorption coefficient of the samples.

pulse repetition rates. The "fast"process causes the matter density to vary due to acoustic wave propagation after local heating. An acoustic wave generated by nonlinear absorption spreads through the beam waist and decreases the refractive index. In the case of nanosecond laser pulses the acoustic waves thus produced are fast enough to interact with the trailing edge of the pulses and cause thermal lensing[46].

5. Spatial self-phase modulation (SSPM)

A wide range of spatial effects can be observed when an intense light beam interacts with a nonlinear medium[44,47–52]. In particular, a concentric ring intensity distribution pattern can be produced in the far field after the beam propagates through a nonlinear material. This phenomenon, known as spatial self phase modulation (SSPM), results

Table 2
The nonlinear absorption coefficient β_{eff} and other parameters for the samples excited using 7 ns laser pulses.

Linear Transmission (LT)	α_0 (cm^{-1})	Energy (μJ)	β_{eff} ($\times 10^{-8}$ cm/W)
25 %	13.86	5	2.2
		10	4.5
		15	4.5
		20	3.7
50 %	7.34	5	1.2
		10	2.5
		15	2.9
		20	1.9
70 %	3.57	5	0.75
		10	0.89
		15	0.95
		20	0.82

from the intensity-dependent complex refractive index and has been observed across several systems, including atomic vapors, liquid crystals, polymers, and nanostructured materials[44,48–50]. Fig. 11 shows the experimental setup for Spatial Self-Phase Modulation (SSPM).

At higher powers and intensities, the refractive nonlinearity of the sample can be better investigated using this technique.

Considering a TEM_{00} Gaussian beam propagating through a nonlinear medium of thickness L along the z-axis, the total phase shift at the exit plane is given by,

$$\varphi(r) = k_o \frac{n_0 r^2}{2R} + \Delta\varphi(r) \tag{14}$$

which comprises of a phase shift arising from the wavefront curvature of the Gaussian beam ($k_0 n_0 r^2/2R$), and also the nonlinear phase shift $\Delta\varphi(r)$. Here k_0 is the free-space wave number, n_0 is the refractive index of the medium, r is the radial coordinate, and R is the radius of wavefront curvature in the corresponding position. The nonlinear phase shift $\Delta\phi(r)$ acquired by the beam due to the intensity-dependent nonlinear refractive index $\Delta n(z,r)$ is given by,

$$\Delta\varphi(\mathbf{r}) = k_o \int_{z_0}^{z_{0+L}} \Delta n(z,r)\,dz \tag{15}$$

where α is the linear absorption coefficient of the medium. The total phase shift φ (r) then becomes,

$$\varphi(r) = k_o \frac{n_0 r^2}{2R} + \Delta\varphi(r) = k_o \left[\frac{n_0 r^2}{2R} + \int_{z_0}^{z_{0+L}} \Delta n(z,r)\,dz\right]$$
$$\approx k_o \frac{n_0 r^2}{2R} + \Delta\varphi_0\,(z_0)\exp\left(-\frac{2r^2}{w_p{}^2}\right) \tag{16}$$

where $\Delta\varphi_0(z_0)$ is the peak nonlinear phase shift at z_0 given by

$$\Delta\varphi_0(z_0) = k_0 \Delta n(z_0,0) L \tag{17}$$

with $\Delta n(z_0,r)$ related to the nonlinear refractive index coefficient n_2 by

$$\Delta n(z_0,r) = n_2 I(z,r) \tag{18}$$

The contributions from the Gaussian and nonlinear phase shifts govern the far field intensity distribution of the diffraction patterns. The far field intensity distribution can be approximated using the Fresnel-Kirchhoff diffraction integral as,

$$I(\rho) = I' \int_0^\infty \left| J_0(k\theta r)\exp\left(-\frac{r^2}{\omega^2} - i\varphi(r)\right)\right|^2 r\,dr \tag{19}$$

where I' is given by

$$I' = 4\pi^2 \left|\frac{E(0,z)\exp\left(-\frac{\alpha L}{2}\right)}{i\lambda D}\right|^2 \tag{20}$$

In the integrand (eqn. (17)), $J_0(x)$ denotes the zeroth order Bessel function of the first kind, D is the distance from the medium exit plane to the far field observation plane, and θ is the far field diffraction angle. The radial coordinate ρ at the observation plane is related to the far field diffraction angle θ by $\rho = D\theta$. For a self-focusing medium ($\Delta\varphi(r) > 0$) in a converging beam ($R < 0$) or the equivalent case of a self-defocusing medium ($\Delta\varphi(r) < 0$) in a diverging beam ($R > 0$), the number of diffraction rings N is proportional to the phase shift by,

Table 3
Nonlinear refractive index coefficient and other relevant parameters for CW excitation.

Linear Transmission (LT)	α_0 (cm^{-1})	L_{eff} (cm)	Power (mW)	I_0 (W/cm^2)	$\Delta\varphi_0$	n_2 ($\times 10^{-6}$ cm^2/W)
50 %	6.93	0.92787	1	152.1	−4.5	−2.66
		0.92787	1.6	243.4	−7.0	−2.59
		0.92787	2	304.3	−7.8	−2.30
		0.92787	3	456.4	−8.5	−1.68
60 %	5.11	0.88254	1	152.1	−3.3	−2.05
		0.88254	1.6	243.4	−4.9	−1.91
		0.88254	2	304.3	−5.9	−1.84
		0.88254	3	456.4	−6.8	−1.41
70 %	3.57	0.80374	1	152.1	−2.5	−1.71
		0.80374	1.6	243.4	−2.8	−1.2
		0.80374	2	304.3	−4.0	−1.37
		0.80374	3	456.4	−5.6	−1.28

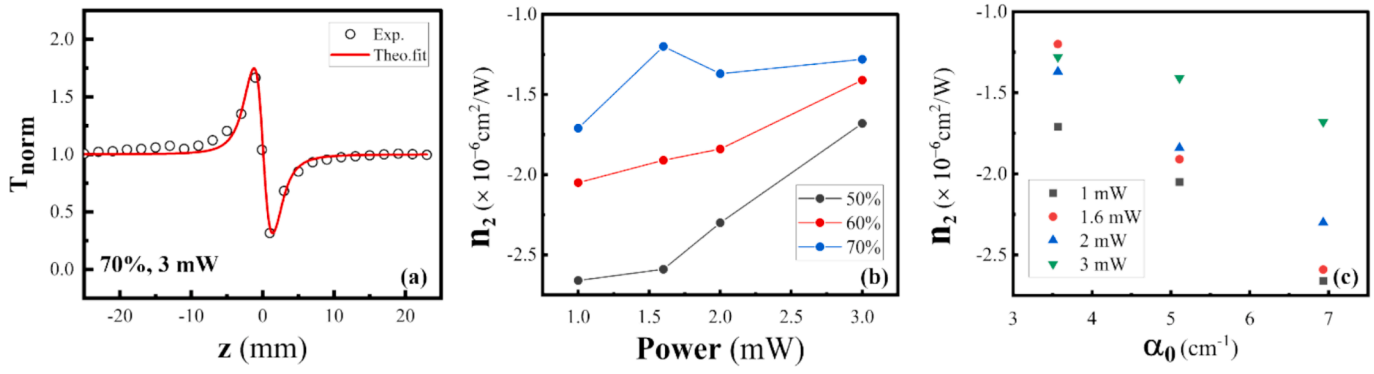

Fig. 9. (a): Closed aperture Z-scan of the dye having LT 70 %, under CW excitation with 3 mW power. **(b):** n_2 plotted as a function of input power for samples with LT values 50 %, 60 % and 70 %, respectively. **(c):** n_2 plotted as a function of linear absorption coefficient of samples at input powers 1 mW, 1.6 mW, 2 mW and 3 mW, respectively.

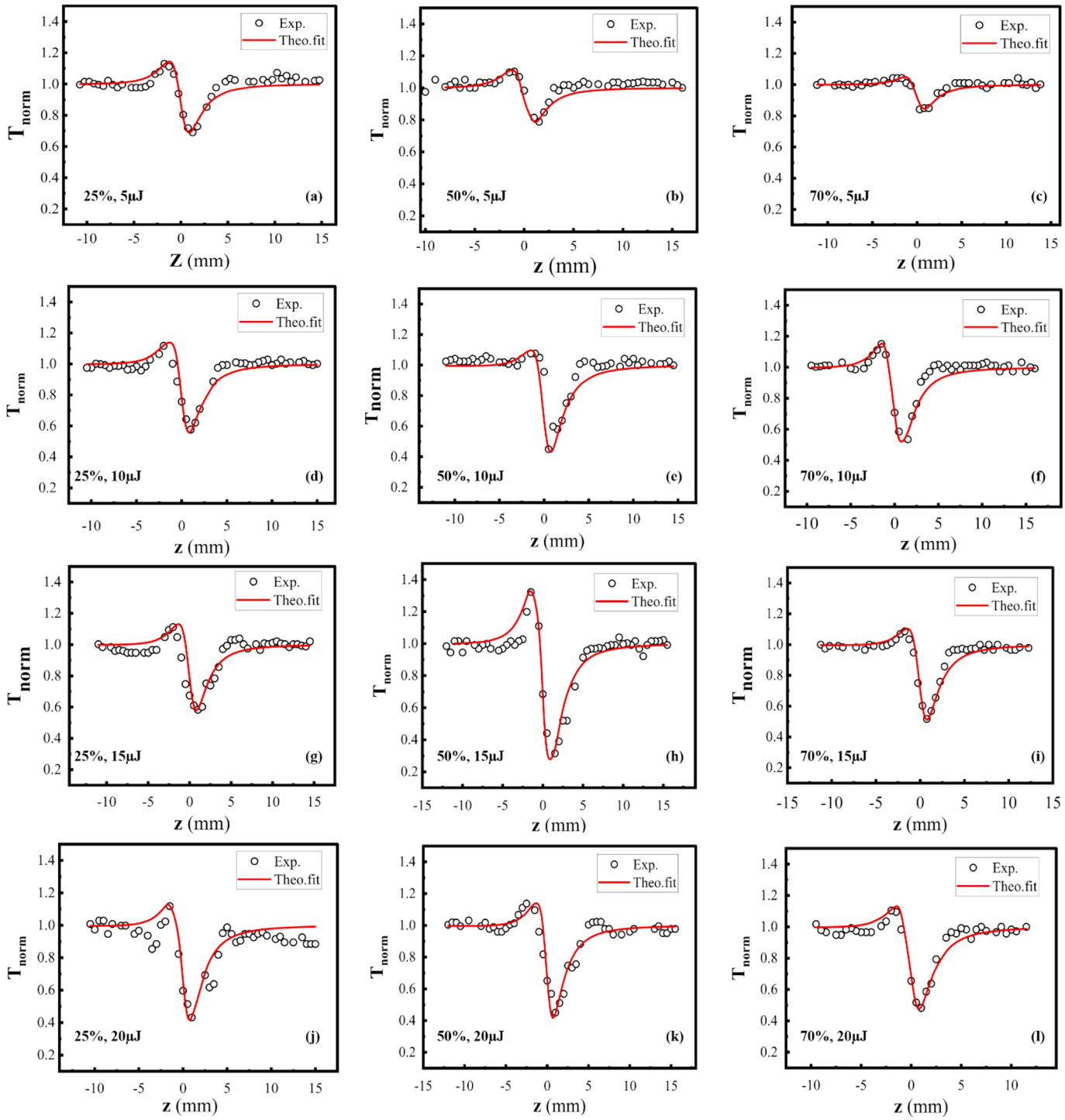

Fig. 10. (a)-(l): Closed aperture Z-scan curves measured in the dye for pulsed (7 ns) excitation. LT values of the samples are 25 %, 50 %, and 70 %, respectively. Laser pulse energies used are 5,10,15, and 20 µJ, respectively.

$$N = \frac{|\Delta\varphi_0|}{2\pi} \tag{21}$$

The nonlinear change in refractive index, Δn_{SSPM} can then be determined using Eqn.17.

Fig. 12 shows the comparison between the measured far field intensity distribution and the corresponding numerical results in a scenario where R < 0 and $\Delta\varphi > 0$. The sample was positioned at a distance of z0 = -0.2 cm from the focal point where R < 0. The images of the diffraction rings captured using a digital camera show that the outermost ring is the thickest, and the distance between concentric rings increases with the radial distance. Notably, all power settings yield a distinct bright centre in the resulting diffraction patterns (see Fig. 12). The presence of a bright or dark spot at the centre is primarily determined by the sign of the product of the phase shift $\Delta\varphi$(r) and the radius of the wavefront curvature R, provided that R is within an appropriate range[43]. With an increase in power, the number of the diffraction rings increases. As can be seen from Fig. 12, the radius of the outer diffraction ring also increases with the input power. The emergence of these diffraction rings can be attributed to the occurrence of SSPM,

Table 4
N_2 , ρ and other relevant parameters for pulsed excitation.

Linear Transmission (LT)	α_0 (cm^{-1})	Energy (μJ)	L_{eff} (cm)	$\Delta\varphi_0$	$\Delta\Psi_0$	ρ	n_2 ($\times10^{-15}$ cm^2/W)
25 %	13.86	5	0.98197	−1.16384	0.197853	−0.17	−3.2
		10	0.98197	−1.49644	0.344181	−0.23	−1.9
		15	0.98197	−1.37424	0.34356	−0.25	−1.4
		20	0.98197	−1.78104	0.534312	−0.3	−1.23
48 %	7.34	5	0.9346	−0.87288	0.139661	−0.16	−2.4
		10	0.9346	−1.6049	0.561715	−0.35	−2.2
		15	0.9346	−2.3985	0.23985	−0.1	−2.25
		20	0.9346	−1.6757	0.50271	−0.3	−1.3
70 %	3.57	5	0.80374	−0.50932	0.12733	−0.25	−1.4
		10	0.80374	−1.67785	0.436241	−0.26	−2.3
		15	0.80374	−1.43875	0.4604	−0.32	−1.25
		20	0.80374	−1.6104	0.467016	−0.29	−1.2

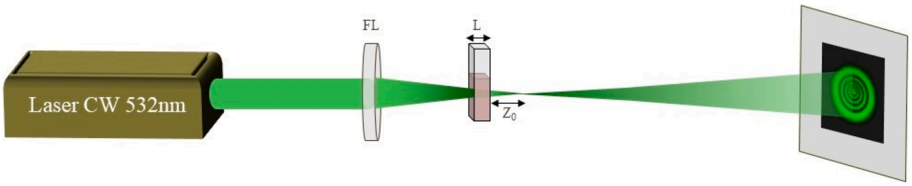

Fig. 11. Experimental layout for Spatial Self Phase Modulation (SSPM) Technique.

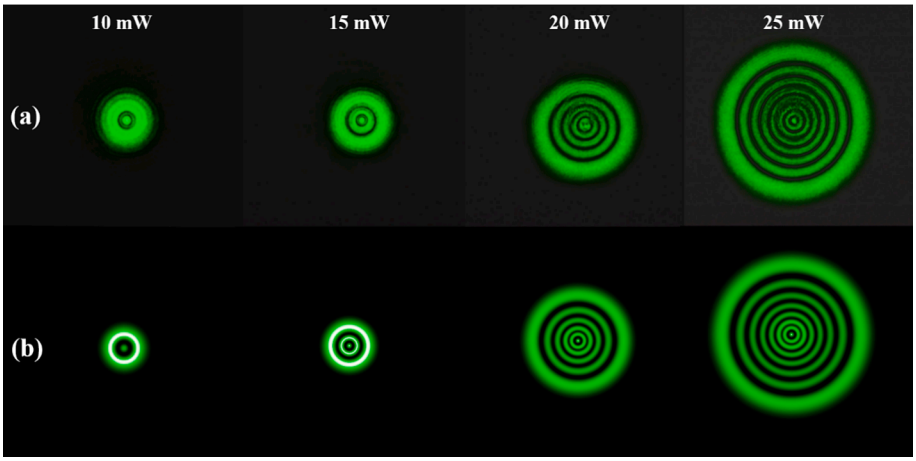

Fig. 12. **(a)** Experimentally measured, and **(b)** numerically simulated diffraction ring patterns for the sample at input powers of 10, 15, 20 and 25 mW, respectively.

originating from the nonlinear optical properties exhibited by the dye solution. From eqns. (18) and (19) it can be seen that the formation of the diffraction rings is independent of the type of nonlinearity, provided an intensity dependent nonlinear refractive index distribution forms in the sample under laser irradiation. In the current experiment the formation of diffraction rings is largely due to the thermally induced nonlinear refraction. The thermally induced change in refractive index can be written as [53]

$$\Delta n_{thermal} = \frac{\partial n}{\partial t}\frac{I\alpha\omega^2}{4K} \tag{22}$$

where $\frac{\partial n}{\partial t}$ is the thermo-optic coefficient, I the optical intensity, α the linear absorption coefficient, ω the beam radius, and K the thermal conductivity. Using the value 5×10^{-4} K^{-1}as the thermo-optic coefficient of DMSO[50], the change in refractive index ($\Delta n_{thermal}$) can be calculated. This value is found to be in close agreement with the Δn_{SSPM} obtained from the number of diffraction rings. This confirms that the diffraction ring formation occurs primarily from thermally induced nonlinear refraction. Values of Δn_{SSPM} and $\Delta n_{thermal}$ calculated for different laser powers from the diffraction rings are given in Table 5.

It is worthwhile to note that the β_{eff} and n_2 values obtained for the *Tectona Grandis L.f.* leaf extract are comparable to those reported in literature for efficient NLO materials. Comparisons to literature values is shown in Tables 6 and 7 respectively.

6. Conclusion

The natural dye present in *Tectona Grandis L.f.* leaves is extracted by ultrasonication and centrifugation of the leaf powder in DMSO. Absorption, excitation and emission spectra of the dye have been measured. Nonlinear optical measurements have been carried out using

Table 5
Measured values of linear transmittance, input power, number of diffraction rings, nonlinear refractive index coefficient, Δn_{SSPM} and $\Delta n_{thermal}$.

Linear Transmission	Power (mW)	N	Δn_{SSPM} ($\times10^{-4}$)	$\Delta n_{thermal}$ ($\times10^{-4}$)
0.5	10	1	−5.36	−9.36
	15	2	−10.74	−14.04
	20	5	−26.75	−18.72
	25	7	−37.39	−23.41

Table 6
β_{eff} and n_2 values reported in literature for different materials under cw laser excitation.

Material	β_{eff} (cm/W)	n_2 (cm^2/W)	References
Fast green FCF dye	6.5×10^{-5}	-3.2×10^{-8}	[54]
Basic violet 16 dye	-1.38×10^{-3}	-2.81×10^{-8}	[55]
Semiconductor ZnS nanoparticles	-3.2×10^{-3}	-1.38×10^{-8}	[56]
Polymer nanocomposite films	45.5×10^{-2}	-2.75×10^{-7}	[57]
C1A1-phthalocyanine	1.3×10^{-3}	-18×10^{-8}	[58]
Tris(acetylacetonato) manganese(III)	1.2×10^{-2}	-1.17×10^{-7}	[59]
Tectona Grandis *L.f* (Teak)	$3.5–16 \times 10^{-3}$	$-(0.75–4.5) \times 10^{-8}$	[current work]

Table 7
β_{eff} and n_2 values of different materials reported in literature for pulsed laser excitation.

Sl. no.	Sample	Laser & measurement parameters	β (m/W)	n_2 (cm^2/W)	References
1.	Se–Te nanorods	5 ns, 532 nm, LT = 75 %, *L* = 1 mm	8.1×10^{-11}		[60]
2.	PbS microtowers	5 ns, 532 nm, LT = 75 %, *L* = 1 mm	10^{-11}–10^{-10}	–	[61]
3.	Graphene oxide	5 ns, 532 nm, LT = 50 %, *L* = 1 mm	3.5×10^{-10}	9.74×10^{-14}	[63]
4.	Graphene oxide–Fe3O4	5 ns, 532 nm, LT = 49 %, *L* = 5 mm	2.6×10^{-10}	2.83×10^{-13}	[63]
5.	Indigofera Tinctoria leaves	5 ns, 532 nm, LT = 70 %, *L* = 1 mm	5.5×10^{-10}	10^{-13} to 10^{-14}	[16]
6.	Tectona Grandis *L.f* (Teak)	5 ns, 532 nm, LT = 62 %, *L* = 1 mm	4.5×10^{-10}	3.2×10^{-15}	[current work]

CW and pulsed lasers at the wavelength of 532 nm. Open aperture Z-scan measurements reveal that the dye shows an excellent optical limiting behaviour (RSA), which originates primarily from excited state absorption. Closed aperture Z-scan measurements show negative nonlinear refraction (n_2) which originates from thermally induced self-defocusing of the beam. SSPM measurements were used to measure n_2 for higher input laser powers. Under CW excitation, the nonlinear absorption coefficient is found to lie in the range 3.0×10^{-3} to 16×10^{-3} cm/W, and the nonlinear refractive index is in the range -1.2×10^{-6} to -2.66×10^{-6} cm^2/W. The corresponding values for pulsed excitation are in the range 0.75×10^{-8} to 4.5×10^{-8} cm/W, and 1.2×10^{-15} to 3.2×10^{-15} cm^2/W, respectively. The experimental result shows that the natural dye extracted from teak leaves can be an efficient optical limiter to prevent damage to sensors and human eyes from laser radiation.

CRediT authorship contribution statement

Beryl C.: Writing – original draft, Methodology, Investigation, Formal analysis, Conceptualization. **Amogh M.S.:** Writing – original draft, Software, Investigation, Formal analysis. **Cyril Benny:** Software, Investigation. **P.R. Biju:** Writing – review & editing, Supervision, Methodology. **Reji Philip:** Writing – review & editing, Supervision, Conceptualization.

Declaration of competing interest

The authors declare that they have no known competing financial interests or personal relationships that could have appeared to influence the work reported in this paper.

Acknowledgments

Authors thank K.N. Vasudha, Raman Research Institute, for her assistance with the UV-VIS and FTIR spectroscopic measurements. Beryl C. acknowledges the Department of Science and Technology (DST), Government of India, for the financial support through the WOS-A grant (no. DST/WOS-A/PM-97/2021).

Appendix A. Supplementary data

Supplementary data to this article can be found online at https://doi.org/10.1016/j.jphotochem.2024.116258.

Data availability

Data will be made available on request.

References

[1] X. Hu, P. Jiang, C. Ding, H. Yang, Q. Gong, Picosecond and low-power all-optical switching based on an organic photonic-bandgap microcavity, Nat. Photon. 2 (2008) 185–189.
[2] R. Hagen, T. Bieringer, Photoaddressable polymers for optical data storage, Adv. Mater. 13 (2001) 1805–1810.
[3] B. Anand, R.Podila, K. Lingam, S.R. Krishnan, S. Siva Sankara Sai, R. Philip, and A. M. Rao, Optical diode action from axially asymmetric nonlinearity in an all-carbon solid-state device. Nano letters, 2013,13(12), pp.5771-5776.
[4] P. Chantharasupawong, R. Philip, N.T. Narayanan, P.M. Sudeep, A. Mathkar, P. M. Ajayan, J. Thomas, Optical power limiting in fluorinated graphene oxide: an insight into the nonlinear optical properties, J. Phys. Chem. C 116 (49) (2012) 25955–25961.
[5] R. Philip, P. Chantharasupawong, H. Qian, R. Jin, J. Thomas, Evolution of nonlinear optical properties: from gold atomic clusters to plasmonic nanocrystals, Nano Lett. 12 (9) (2012) 4661–4667.
[6] S. Webster, J. Fu, L.A. Padilha, O.V. Przhonska, D.J. Hagan, E.W. Van Stryland, M. V. Bondar, Y.L. Slominsky, A.D. Kachkovski, Comparison of nonlinear absorption in three similar dyes: polymethine, squaraine and tetraone, Chem. Phys. 348 (2008) 143.
[7] B. Karthikeyan, C.S. Suchand Sandeep, T. Pandiyarajan, P. Venkatesan, R. Philip, Spectrally broadened excitonic absorption and enhanced optical nonlinearities in Dy 3+-doped ZnO nanoparticles, Appl. Phys. A 102 (2011) 115–120.
[8] Y. Han, Q. Zhuang, X. Chen, W. Ma, H. Lu, H. Song, Doubly 1,3-butadiyne-bridged ditwistacene with enhanced ultrafast broadband reverse saturable absorption, J Mater Chem c. 10 (38) (2022) 14122–14127.
[9] Y. Han, J. Xiao, X. Wu, Y. Wang, X. Zhang, Y. Song, Excellent ultrafast broadband optical limiting of functionalized twistacenes based on two-photon absorption-induced excited state absorption, Dyes Pigm. 208 (2023) 110842.
[10] J. Xiao, S. Wang, T. Ye, Post-Functionalization of End-Capping Twistacenes with Pyrene Units, Org. Chem. Front. 11 (2024) 5638–5669.
[11] P.C. Haripadmam, C. Beryl, Reji Philip, Optical Limiting Properties of the Natural Dye Extract from Alternanthera brasiliana Leaves, J. Electron. Mater. 51 (7) (2022) 3364–3371.
[12] L.R. Dalton, Organic electro-optic materials, Pure Appl. Chem. 76 (2004) 1421–1433.
[13] S.R. Marder, Organic nonlinear optical materials: where we have been and where we are going, Chem. Commun. 131–134 (2006).
[14] B. Anand, N. Roy, S. Siva Sankara Sai, Reji Philip, Spectral dispersion of ultrafast optical limiting in Coumarin-120 by white-light continuum Z-scan. Applied Physics Letters, 2013, 102(20).
[15] R. Mansour, Natural dyes and pigments: extraction and applications, Handbook of Renewable Materials for Coloration and Finishing, John Wiley & Sons (2018) 75–102.
[16] C.D. Beryl, N. Reji, R. Philip, Optical limiting behavior of the natural dye extract from indigofera Tinctoria leaves, Opt. Mater. 114 (2021) 110925.
[17] P. Haripadmam, T. Thanuja, G. Varsha, C. Beryl, A. Aji, Nonlinear optical absorption in PVA films doped by the novel natural dye extract from C, Redflash Leaves. Optical Materials 112 (2021) 110804.
[18] M. Sheik-Bahae, A.A. Said, E.W. Van Stryland, High-sensitivity, single-beam n 2 measurements, Opt. Lett. 14 (17) (1989) 955–957.
[19] M. Sheik-Bahae, A.A. Said, T.H. Wei, D.J. Hang, E.W. Van Stryland, Sensitive measurement of optical nonlinearities using a single beam, IEEE J. Quant. Electr. 26 (1990) 760.
[20] T.K. Kopa, et al., Antiplasmodial anthraquinones and hemisynthetic derivatives from the leaves of Tectona grandis (Verbenaceae), *Phytochem. Lett.* 8 (2014) 41–45.
[21] F. A. Macías, R. Lacret, R. M. Varela, C. Nogueiras, and J. M. G. Molinillo, 'Bioactive apocarotenoids from Tectona grandis', *Phytochemistry*, 2008, vol. 69, no.

15, pp. 2708–2715, [22] A. M. Aguinaldo, O. P. M. Ocampo, B. F. Bowden, A. I. Gray, and P. G. Waterman, 'Tectograndone, an anthraquinone-naphthoquinone pigment from the leaves of Tectona grandis', *Phytochemistry*, 1993, 33, 933–935.
[22] R. Lacret, R.M. Varela, J.M.G. Molinillo, C. Nogueiras, F.A. Macías, Tectonoelins, new norlignans from a bioactive extract of Tectona grandis, *Phytochem. Lett.* 5 (2012) 382–386.
[23] A.H. Ahliha, F. Nurosyid, A. Supriyanto, T. Kusumaningsih, The chemical bonds effect of anthocyanin and chlorophyll dyes on TiO2 for dye-sensitized solar cell (DSSC), J. Phys. Conf. 909 (2017) 012013.
[24] W.A. Ayalew, D.W. Ayele, Dye-sensitized solar cells using natural dye as light-harvesting materials extracted from Acanthus sennii chiovenda flower and Euphorbia cotinifolia leaf, J. Sci.: Adv. Mat. Dev 1 (2016) 488–494.
[25] A.R. Hernandez-Martínez, M. Estevez, S. Vargas, F. Quintanilla, R. Rodríguez, Natural pigment based dye sensitized solar cells, J. Appl. Res. Technol. 10 (2012) 38–47.
[26] H.J. Kim, Y.T. Bin, S.N. Karthick, K.V. Hemalatha, C. Justin Raj, S. Venkatesan, Songyi Park, G. Vijayakumar, Natural dye extracted from Rhododendron species flowers as a photosensitizer in dye sensitized solar cell, Int. J. Electrochem. Sci. 2013, 8, 6734-6743.
[27] B. Pliszka, T. Olszewska, R. Drabent, Fluorescence of anthocyanin pigments in plant extracts at various pH, Proc. SPIE 4515, Light and Optics, Biomedicine (2001).
[28] C. Albrecht, R. Joseph Lakowicz, 2008, Principles of fluorescence spectroscopy.
[29] N. Mozhzhukhina, L.P. Méndez, D.e. Leo, E.J. Calvo, Infrared Spectroscopy Studies on Stability of Dimethyl Sulfoxide for Application in a Li–Air Battery, J. Phys. Chem. C 117 (36) (2013) 18375–18380.
[30] R. Kushwaha, P. Srivastava, L. Bahadur, Natural Pigments from Plants Used as Sensitizers for TiO2 Based Dye-Sensitized Solar Cells, Journal of Energy (2013).
[31] J. Coates, Interpretation of infrared spectra: A practical approach, in: R.A. Meyers (Ed.), Encyclopedia of Analytical Chemistry, John Wiley & Sons Ltd., 2000, pp. 10815–10837.
[32] V. Pereira Jr , Aniceto, Arruda, I.N. Queiroz de, S. Ricardo, Active chitosan/PVA films with anthocyanins from Brassica oleraceae (Red Cabbage) as Time-Temperature Indicators for application in intelligent food packaging, Food Hydrocolloids, 2015, 43, 180-188.
[33] D. Tahir, R. Abidin, P. Gareso, High Efficiency Dye Sensitized Solar Cell from Tectona Grandis and red Crysanthemum Morifolium as a Sensitizer, IOP Conf. Ser.: Earth Environ. Sci 279 (012031) (2019).
[34] R.L. Sutherland, Handbook of Nonlinear Optics, CRC Press, Boca Raton, USA, 2003.
[35] S. Pramodini, P. Poornesh, Third-order nonlinear optical response of indigo carmine under 633nm excitation for nonlinear optical applications, Opt. Laser Technol. 63 (2014) 114–119.
[36] M. Rumi, J.W. Perry, Adv. Opt. Photonics 2 (2010) 451.
[37] R. Philip, G.R. Kumar, N. Sandhyarani, T. Pradeep, T. "Picosecond optical nonlinearity in monolayer-protected gold, silver, and gold-silver alloy nanoclusters." *Physical Review B*, 2000, 62, 13160–13166.
[38] A. Gaur, H. Syed, B. Yendeti, V.R. Soma, Experimental evidence of two-photon absorption and its saturation in malachite green oxalate: A femtosecond Z-scan study, *J. Opt. Soc. Am. B* 35 (4) (2018) 780–785.
[39] R. Podila, B. Anand, J.P. West, R. Philip, S.S.S. Sai, J. He, M. Skove, S.-J. Hwu, S. Tewari, A.M. Rao, Nanotechnology 22 (2011) 095703.
[40] F. Cuppo, A. Figueiredo Neto, S. Gómez, P. Palffy-Muhoray, Thermal-lens model compared with the Sheik-Bahae formalism in interpreting Z-scan experiments on lyotropic liquid crystals, J. Opt. Soc. Am. B 19 (2002) 1342–1348.
[41] M. Konstantaki, E. Koudoumas, S. Couris, P. Lainé, E. Amouyal, S. Leach, Substantial non-linear optical response of new polyads based on Ru and Os complexes of modified terpyridines, J. Phys. Chem. B 105 (44) (2001) 10797–10804.
[42] A. Santhi, Vinu V. Namboodiri, P. Radhakrishnan, V. P. N. Nampoori, Simultaneous determination of nonlinear optical and thermo-optic parameters of liquid samples, Appl. Phys. Lett. 89, 2006, 231113.
[43] R. W. Boyd, (2020). Nonlinear Optics (4th ed.). Academic Press.
[44] X. Liu, S. Guo, H. Wang, L. Hou, Theoretical study on the closed-aperture Z-scan curves in the materials with nonlinear refraction and strong nonlinear absorption, Opt. Commun. 197 (4–6) (2001) 431–437.
[45] R.A. Ganeev, A.I. Ryasnyansky, M. Baba, M. Suzuki, N. Ishizawa, M. Turu, H. Kuroda, Nonlinear refraction in CS_2, Appl. Phys. B 78 (2004) 433–438.
[46] J. H. Marburger, J. Opt. Soc. Am. B 7 (1990) – Special issue on transverse effects in nonlinear optics.
[47] D.J. Harter, R.W. Boyd, Four-wave mixing resonantly enhanced by ac-Stark-split levels in self-trapped filaments of light, Phys Rev. A 29 (1984) 739–748.
[48] J. J. Wu, Shu-Hsia Chen, J. Y. Fan, and G. S. Ong, "Propagation of a Gaussian-profile laser beam in nematic liquid crystals and the structure of its nonlinear diffraction," J. Opt. Soc. Am B 7, 1147-1157 (1990).
[49] E. Snatamato, Y.R. Shen, Field-curvature effect on the diffraction ring pattern of a laser beam dressed by spatial self-phase modulation in a nematic film, Opt. Lett. 9 (1984) 564–566.
[50] J. Robertson, P. Milsom, J. Duignan, G. Bourhill, Spatial redistribution of energy in a nanosecond laser pulse by an organic optical limiter, Opt. Lett. 25 (2000) 1258–1260.
[51] L. Deng, K. He, T. Zhou, C. Li, Formation and evolution of far-field diffraction patterns of divergent and convergent Gaussian beams passing through self-focusing and self-defocusing media, J. Opt. a: Pure Appl. Opt. 7 (2005) 409–415.
[52] K. Ogusu, Y. Kohtani, H. Shao, Laser-Induced Diffraction Rings from an Absorbing Solution, OPT REV 3 (1996) 232–234.
[53] K. Jamshidi-Ghaleh, S. Salmani, M.H.M. Ara, Nonlinear responses and optical limiting behavior of fast green FCF dye under a low power CW HeNe laser irradiation, 2007, Opt. Commun. 271.
[54] M. Rashidian, D. Dorranian, S.A. Darani, S. Saghafi, M. Ghoranneviss, Nonlinear responses and optical limiting behavior of basic violet 16 dye under CW laser illumination, 2009, Optik 120.
[55] Z. Dehghani, S. Nazerdeylami, E. Saievar-Iranizad, M.H.M. Ara, Synthesis and investigation of nonlinear optical properties of semiconductor ZnS nanoparticles, J. Phys. Chem. Solids 72 (2011).
[56] P.G.L. Frobel, S.R. Suresh, S. Mayadevi, S. Sreeja, C. Mukherjee, C.I. Muneera, Intense low threshold nonlinear absorption and nonlinear refraction in a new organic polymer nanocomposite, Mater. Chem. Phys. 129 (2011).
[57] K. Sathiyamoorthy, C. Vijayan, M.P. Kothiyal, Low power optical limiting in ClAl-phthalocyanine due to self defocusing and self phase modulation effects, 2008, Opt. Mater. 31.
[58] F.Z. Henari, A.Y. Ali-Mohamed, Nonlinear refractive index measurement of tris (acetylacetonato) manganese(III) solution, 2008,Opt. Laser Technol. 40.
[59] K. Sridharan, M.S. Ollakkan, R. Philip, T.J. Park, Non-hydrothermal synthesis and optical limiting properties of one-dimensional Se/C, Te/C and Se–Te/C core–shell nanostructures, Carbon 63 (2013) 263–273.
[60] T.V. Tamilselvan, K.S. Kishore, K.N. Rao, R.P. Reji, Optical nonlinearity in lead sulfide microtowers, J. Phys. d: Appl. Phys. 43 (2010) 385402.
[61] X.-L. Zhi, X. Zhi, Z.-B. Liu, S. Shuo, W.-Y. Zhang, J.-G. Tian, et al., Nonlinear optical and optical limiting properties of graphene oxide–Fe3O4 hybrid material, *J. Opt.* 13 (2011) 075202.